J. Fluid Mech. (1983), *vol.* 129, *pp.* 91–108
Printed in Great Britain

Axisymmetric meniscus formation: a viscous-fluid model for cones

By P. T. SQUIRE
School of Physics, University of Bath, England

(Received 6 April 1982)

The dynamics of the formation of the axisymmetric meniscus around a cone contacting a free liquid surface are discussed. An approximate phenomenological model is set up. In the case considered, where $Re \ll 1$ and viscosity dominates the retarding forces, this leads to a differential equation relating the height of the circle of contact to time. Solutions are derived, involving one or more unknown parameters, which describe the time dependence of the height of the circle of contact.

Experimental data, obtained from delayed flash photographs of the meniscus profiles of silicone fluid climbing over the surface of glass cones, provide general support for the model. The agreement between the predicted and observed height as a function of time is sufficiently close to justify the model as a useful description.

1. Introduction

When a solid body makes contact with a liquid that wets it, a meniscus is formed. The shape of this meniscus when fully formed depends on the surface tension and density of the liquid, the shape of the solid and the contact angle between liquid and solid. Except in very special cases even the final shape of the meniscus cannot be expressed analytically. However, extensive numerical calculations of this final static profile have been made since the pioneering paper of Bashforth and Adams (1883). A recent review has been given by Padday (1976). Comprehensive tables of static profiles have been published by Hartland & Hartley (1976).

Less has been published about the growth of such a meniscus from the moment of first contact between solid and liquid, though studies have been made of the rise of the constrained meniscus in capillary tubes (e.g. Kissling & Gross 1970; Huh & Mason 1977).

In this paper the dynamics of meniscus formation for a cone making contact with the free surface of a viscous liquid are considered. More specifically the paper treats the problem illustrated in figure 1, which shows a cone with its axis vertical making contact with a horizontal liquid surface. Figure 1(*a*) shows the situation at the moment of contact. Figures 1(*b–d*) show the evolution of the fully formed static meniscus. In this paper the balance of forces associated with the motion is used to derive a simple physical model as a basis for the presentation of experimental results. In particular, an equation is derived for the time dependence of the height of the circle of contact between the meniscus and the cone, for the case when the inertial terms in the force-balance equation are negligible.

The experimental part of the paper describes how the height of the meniscus and other aspects of its shape have been observed. Detailed results are presented of height as a function of time for various values of cone angle and liquid viscosity.

The objective of the work is to establish an approximate theoretical model for the phenomenon, and to evaluate it against detailed experimental data.

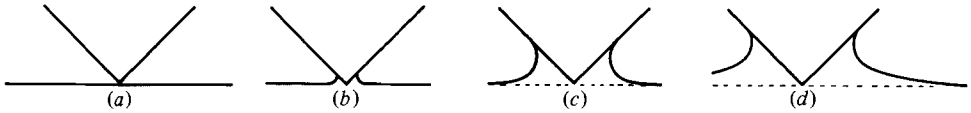

FIGURE 1. Evolution of static meniscus from moment of contact.

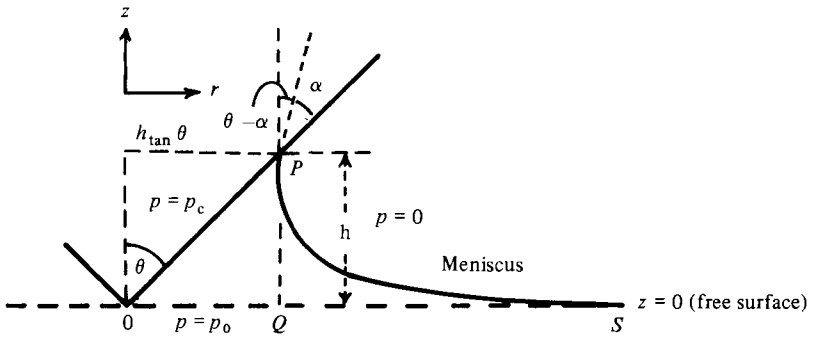

FIGURE 2. Section through cone and meniscus, defining coordinates of model. See text for details.

2. Formulation of a semi-empirical model

2.1. *Basic assumptions*

Figure 2 shows an axial section through the cone and the meniscus. All pressures are measured relative to that of the atmosphere.

A rigorous treatment of the problem starting with the Navier–Stokes equations is beset by a number of severe difficulties, notably the following.

(*a*) The behaviour of an advancing contact line between liquid and solid is not well understood. In particular the variation of contact angle with time cannot be calculated.

(*b*) The upper, curved surface of the meniscus forms a moving boundary whose shape as a function of time is both a condition and the goal of the solution.

(*c*) The fluid motion in the liquid below the free surface depends on the size and shape of the boundaries of the container. Ideally the experiments would be carried out in a infinite reservoir of liquid; in practice finite containers must be used.

(*d*) Viscous drag of partially immersed bodies is not well understood.

(*e*) For the general case inertial terms in the Navier–Stokes equation lead to mathematical difficulties.

In the approximate model developed here a number of simplifying assumptions will be made which enable some of these difficulties to be circumvented. The objective is to provide a framework for the presentation and discussion of the detailed experimental results in §4. The initial assumptions are as follows.

(i) Details of the motion of the liquid below the free surface may be neglected so far as its effect on the meniscus is concerned.

(ii) Viscous drag may be described by a single dimensionless parameter in a manner analogous to drag at uniform velocity in a homogeneous fluid. This is supported by a recent study of impact drag (Moghisi & Squire 1981).

(iii) The liquid viscosity is sufficiently high to justify neglect of the time-derivative terms in the equation of motion. This is the fundamental assumption of all creeping motion calculations.

2.2. *Force balance*

For the case of low-Reynolds-number flow the balance of forces acting on the liquid volume V bounded by the cone, the meniscus and the free surface $z = 0$ (figure 2) may be expressed as

$$F_\sigma + F_p + F_g + F_v = 0, \tag{1}$$

where the terms denote vertical force components corresponding to the following physical effects:

F_σ – surface tension along the circle of contact;

F_p – hydrostatic pressure acting on submerged surface of the cone;

F_g – gravity;

F_v – viscous drag.

Explicit expressions will now be derived for each of these in terms of the height h of the circle of contact.

Surface-tension force F_σ. This is the cause of the upward motion, and may be written exactly if the contact angle α is known. The vertical component of the surface tension force along the line of contact (figure 2) is given by

$$F_\sigma = 2\pi\sigma \tan\theta \cos(\theta - \alpha)\, h, \tag{2}$$

where σ is the surface tension and θ is the semivertical angle of the cone.

There is a major difficulty in evaluating (2) because α is the *dynamic* contact angle. Although many studies have been made of the contact angle for moving contact lines (Dussan V. 1979), it is still not possible to specify α with any confidence for such problems. Nor is it straightforward to derive it from photographs. The main difficulty arises in deciding at which point to measure α, since when the contact line is moving there is a pronounced distortion of the interface within a very small distance from the contact line. It is quite possible, for example, that α is zero at the contact line, but signifiantly different from zero at a distance too small to be seen on the photographs. In other words, the *apparent* contact angle may differ appreciably from the actual contact angle (Hansen & Toong 1971).

For this reason α will be retained in (2) as an unknown parameter. It can then be incorporated either on the basis of improved theoretical understanding or of experimental information.

Pressure term F_p. The curvature of the meniscus causes a reduction in pressure above the free surface. In the static case this is just balanced by the hydrostatic pressure $-\rho g z$. It is assumed that the pressure has the hydrostatic value, so that the upward force on the liquid is

$$\begin{aligned} F_p &= \rho g \int_0^h 2\pi \tan^2\theta\, z^2\, dz \\ &= \tfrac{2}{3}\pi\rho g \tan^2\theta\, h^3. \end{aligned} \tag{3}$$

Gravitational force F_g. The downward gravitational force is given by

$$F_g = -\rho g V. \tag{4}$$

The problem is to relate the meniscus volume V to the height h. Since even the static profile cannot be expressed analytically it is unrealistic to seek an exact expression for $V(h)$. In seeking an approximate expression for $V(h)$ either an assumption about the meniscus shape must be made or empirical evidence is needed. Two alternative assumptions will be considered here. In §4 experimental observations of $V(h)$ will be presented.

The simplest assumption that can be made concerning V is that the meniscus shape is constant throughout its formation. It then follows dimensionally that

$$V = kh^3, \tag{5}$$

where k is a dimensionless constant which must be chosen to satisfy the final static meniscus height and volume; that is

$$V_\infty = kh_\infty^3. \tag{5a}$$

V_∞ and h_∞ can be found from numerical integration of the Young–Laplace equation. The details of this are given in the appendix. k is thereby determined for a particular cone angle.

In the absence of a rigorous treatment of the dynamic meniscus profile, the next simplest assumption that can realistically be made is that the static shape is found everywhere except very close to the contact line. A short-range adjustment in the surface can then allow the actual contact angle to be zero, as explained above in the discussion of F_σ. It is then possible to calculate the meniscus volume $V(h)$ from the static profiles. The details of the calculation are also given in the appendix. Typical results are shown in figure 14.

For the purposes of setting up the governing equation for the meniscus height, it will be convenient to leave the volume specified as $V(h)$. The equations may then be integrated using either the values calculated from the static profiles or the measured values.

Viscous drag F_ν. Exact expressions for the drag force on partially immersed bodies are not available. The drag force on a sphere during impact with an inviscid liquid has been extensively studied both theoretically (e.g. Miloh 1981) and experimentally (e.g. May & Woodhall 1948). The impact of a cone has also been studied, though less extensively (Shiffman & Spencer 1951; Watanabe 1930). These studies all relate to the case of a moving solid and an inviscid liquid. The case of impact on a viscous liquid has recently been studied by Moghisi & Squire (1981), who showed that for a sphere the impact drag force may be represented by an expression of the form

$$F_{\mathrm{D}} = \tfrac{1}{2} C_{\mathrm{D}} \rho A v^2, \tag{6}$$

where A is the cross-sectional area and v is the impact velocity. The impact drag coefficient C_{D} may be expressed in the form

$$C_{\mathrm{D}} = \frac{a}{Re} \quad (Re \ll 1), \tag{7}$$

where a depends on the depth of immersion.

Equations (6) and (7) will be recognized as the familiar expressions for the drag force on a body moving at constant velocity in a homogeneous fluid at low Reynolds number: so-called Stokes drag. The only difference is the value of the constant of proportionality a between the drag coefficient and inverse Reynolds number (7). For the homogeneous case $a = 24$, while for the impact case a is a function of the depth of immersion, involving only one or two parameters during the early stages of impact.

This result suggests that it may be possible to describe the viscous drag force for the present problem by a single parameter. The cases of moving solid and moving

liquid are not generally equivalent, but in the special case of creeping motion ($Re \ll 1$) they are. Thus the meniscus drag force will be written by analogy with (6) as

$$F_v = -\tfrac{1}{2}C_D \rho A v^2, \tag{8}$$

$$A = \pi(h \tan\theta)^2, \tag{9}$$

$$v = \frac{dh}{dt}. \tag{10}$$

Also, by analogy with (7) the drag coefficient will be written as

$$C_D = \frac{b}{Re}. \tag{11}$$

The Reynolds number will be taken as

$$Re = \frac{2\pi h \tan\theta\, v}{\nu}. \tag{12}$$

Equations (8)–(12) combine to give

$$F_v = -(\tfrac{1}{4}b\rho\nu \tan\theta)\, h \frac{dh}{dt}. \tag{13}$$

It should be noted that b cannot be calculated theoretically at present, and so must be regarded as an adjustable parameter to be determined by experiment.

2.3. *The governing equation for $h(t)$*

The force-balance equation may now be written by combining (1)–(4) and (13). After division by $\frac{1}{4}b\nu\rho h \tan\theta$ the result is

$$\frac{dh}{dt} + \frac{4g}{b\nu}\left\{\frac{V(h)}{h\tan\theta} - \tfrac{2}{3}\pi h^2 \tan\theta\right\} = \frac{8\pi\sigma\cos(\theta-\alpha)}{b\nu\rho}. \tag{14}$$

Equation (14) is the governing equation for meniscus height as a function of time. In order to integrate it $V(h)$ and α must be specified, as discussed in §2.2. The detailed results of integration will be given in §5.3. However, it is useful to note that the simplest form of $V(h)$, given by (5), enables (14) to be integrated exactly in the convenient form

$$h = h_\infty \tanh\frac{t}{\tau}, \tag{15}$$

where

$$h_\infty = \left\{\frac{\pi\sin\theta}{k - \tfrac{2}{3}\pi\tan^2\theta}\right\}^{\frac{1}{2}}\lambda, \tag{16}$$

$$\tau = \frac{b\nu}{4g\lambda\{\pi\cos\theta\,(k\cot\theta - \tfrac{2}{3}\pi\tan\theta\}^{\frac{1}{2}}}. \tag{17}$$

In (16) and (17) λ is the capillary constant:

$$\lambda = \left(\frac{2\sigma}{\rho g}\right)^{\frac{1}{2}}. \tag{18}$$

2.4. *Dimensionless groups*

There are two distinct dimensionless groups that apply to the meniscus rise. During the early part of the rise the gravitational force F_g and pressure force F_p are small

compared with the surface-tension force F_σ and viscous drag force F_ν. In (14) this corresponds to neglect of the terms in curly brackets on the left-hand side. The motion is then at constant speed,

$$v_0 = \left.\frac{dh}{dt}\right|_0 = \frac{8\pi\sigma\cos\theta}{b\nu\rho}. \tag{19}$$

The dimensionless group that determines whether (19) applies is the Reynolds number

$$Re = \frac{lv}{\nu},$$

where l is a characteristic length and v is the velocity. For the present problem v may be taken as dh/dt. The characteristic length is not constant as the meniscus rises. If it is taken to be the diameter of the circle of contact then $l = 2h\tan\theta$ and

$$Re = \left(\frac{2\tan\theta}{\nu}\right)h\left(\frac{dh}{dt}\right). \tag{20}$$

The transition from inertia-dominated to viscous flow will occur when $Re \approx 1$. Equation (19) is expected to apply when $Re \ll 1$.

When the gravitational term becomes significant there is a dimensionless group, the Suratman number (Catchpole & Fulford 1966), which applies; if the characteristic length is taken to be the capillary constant λ, then

$$Su = \left(\frac{2\sigma^3}{g\nu^4\rho^3}\right)^{\frac{1}{2}}. \tag{21}$$

Physically Su is the ratio of (inertia force × surface-tension force) to the square of the viscous force.

It follows that in performing experiments to measure $h(t)$ similarity between curves may exist in one region but not necessarily in the other. The measurements reported in §4 are mostly in the high-viscosity range for which $Re \ll 1$ and $Su \lesssim 1$.

3. Apparatus for the observation of meniscus formation

The obvious method of observing the formation of a meniscus is by means of high-speed cinéphotography. However, there are several reasons why this method has not been used for the observations reported here. First, the resolution of high-speed ciné film is poor. Secondly, the meniscus rise is highly nonlinear against time. Thus a rapid frame rate is required early in the process and a much slower rate later on; such variable frame rates are not practicable with standard high-speed cameras. Thirdly, it is difficult to couple a high-speed camera to a microscope to obtain the magnification necessary. Fourthly, it is difficult to synchronize the start of the event with a high-speed camera running for perhaps only a second. Finally, the cost of the large number of films required would be prohibitive.

For these reasons a delayed-flash system has been devised for obtaining single exposures on 35 mm film at accurately known times after the moment of contact. The system is shown schematically in figures 3 and 4.

Briefly, the system operates as follows: light from a He–Ne laser is directed within the liquid to undergo total internal refection at the point of contact between the cone and the liquid (figure 3). Before the cone touches the surface the light falls symmetrically on a two-element photodiode (Centronic LD2-5T) connected in series opposition so that the output is initially zero. As soon as contact is made by the cone

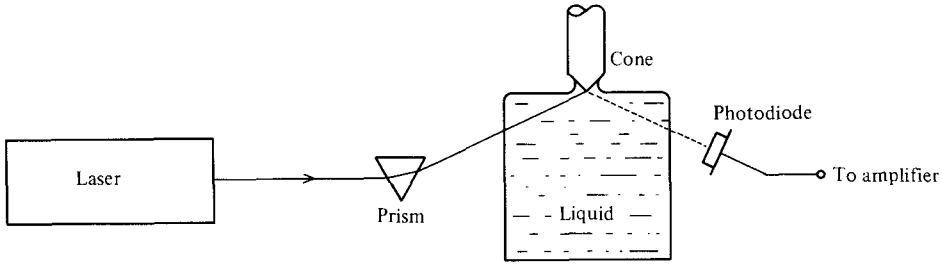

FIGURE 3. Optical triggering system for delayed flash photography.

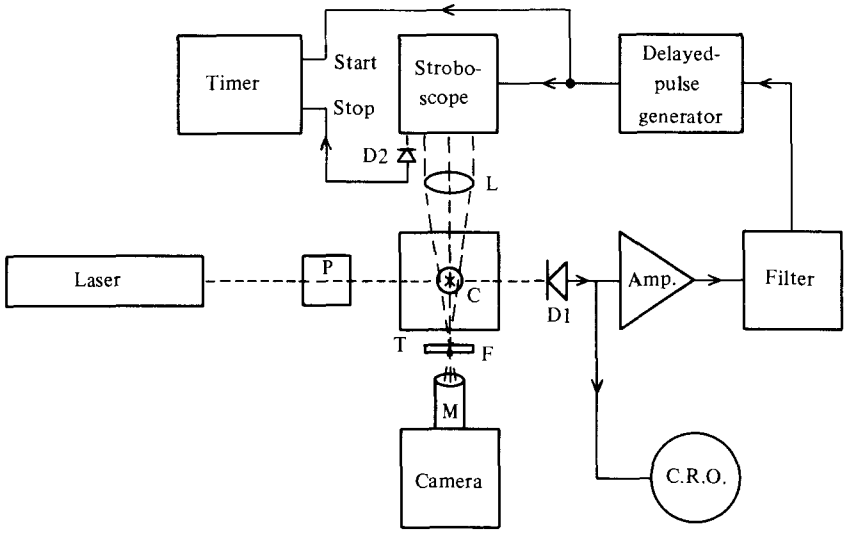

FIGURE 4. Schematic diagram of apparatus for delayed-flash photography. C, cone; D1, D2, photodetectors; F, filter to absorb laser light; L, condensing lens; M, microscope; P, prism; T, tank containing liquid.

the reflected beam is displaced, and an output appears across the photodiode. This is amplified and filtered before triggering a delayed-pulse generator and starting a timer (figure 4). After a variable delay the pulse generator triggers the stroboscope, which emits a single flash. This flash stops the timer and the light is partially focused by the condenser lens on to the liquid meniscus. The camera and microscope are arranged directly along the axis of the stroboscope, so that the meniscus is seen in silhouette. By this means adequate exposure can be obtained with short (about 20 μs) flashes and 400 ASA film.

An optical system of triggering has been chosen because the liquids used in this study were silicone fluids (Dow Corning 200). Being non-conducting these rule out the more straightforward electrical triggering which may be used with conducting liquids.

The cones were of glass, ground and polished to an optical finish by carborundum, diamond and alumina. They were mounted on a micromanipulator so that they could be lowered slowly to touch the liquid surface. Cone entry was thus effectively at zero velocity ($< 0{\cdot}1$ mm s^{-1}). Between each entry the cone was very slowly raised to drain as much liquid as possible from it whilst leaving the surface wet.

4. Results

Some examples of meniscus photographs are shown in figure 5. These indicate the quality of the raw data from which meniscus height and shape must be derived. The main difficulties are in distinguishing between the liquid and the cone surface at the line of contact, and in locating the position of the free surface.

The results are primarily in the form of graphs of meniscus height $h(t)$ as a function of time. These are given first for fixed cone angle ($\theta = 45°$) with variable viscosity (figure 6). Log/log scales have been used for these graphs to permit a wide range of times and viscosities to be shown together. Each point on these graphs corresponds to a separate meniscus formation, and the scatter on the graphs partly results from small variations in the position of the cone tip relative to the free surface. The remaining scatter is due to variations in the amount of liquid adhering to the cone after withdrawal and to the uncertainties in measuring the meniscus height from the photographs.

Note the single set of data in figure 6 obtained with water using cinéphotography. These data are not strictly part of the present study, but are useful in determining what constitutes the high-viscosity region. (See §5.)

The second sequence of results is shown in figure 7. These are graphs of $h(t)$ at fixed viscosity ($\nu = 10^3$ mm^2 s^{-1}) for varying cone angle. Linear scales have been used for these graphs.

Finally, information on the shape is given in figure 8. This is a graph of meniscus volume V against height. $V(h)$ is the shape function that appears in (14). The estimation of V from the photographs is even more difficult than that of h, since the meniscus extends to a distance from the axis several times the height, approaching the surface asymptotically. The very small volume during the early part of the rise, and its variation by more than four orders of magnitude over the measured range should be taken into account when assessing these results. The difficulties involved in deriving accurate data precluded a systematic study of how $V(h)$ depends on viscosity and cone angle. It is gratifying to observe, however, that the single point corresponding to the static meniscus, which can be calculated from numerically integrated profiles, agrees closely with the measured volumes. Details of the calculations are given in the appendix.

5. Analysis and discussion of results

The results have been analysed in three stages: (*a*) the initial rise ($h/h_\infty \lesssim 0{\cdot}5$) during which the viscous retarding force dominates; (*b*) the later stage ($h/h_\infty \gtrsim 0{\cdot}5$) during which the gravitational force and viscous force are both significant; and (*c*) the entire range, to test the model equation (14).

5.1. *Initial rise* ($h < 0{\cdot}5h_\infty$)

In §2.4 it was explained that during the early stages of the meniscus formation, in the viscous limit, the contact line should rise at a constant speed given by (19); i.e.

$$v_0 = \frac{8\pi\sigma\cos\theta}{b\nu\rho}.$$

Inspection of figure 6 confirms this prediction. Curves 2–6 possess a linear portion having a slope of unity on the log/log scales employed. For curves 4–6, corresponding to the higher viscosity values, this linearity occurs until the height is almost half the

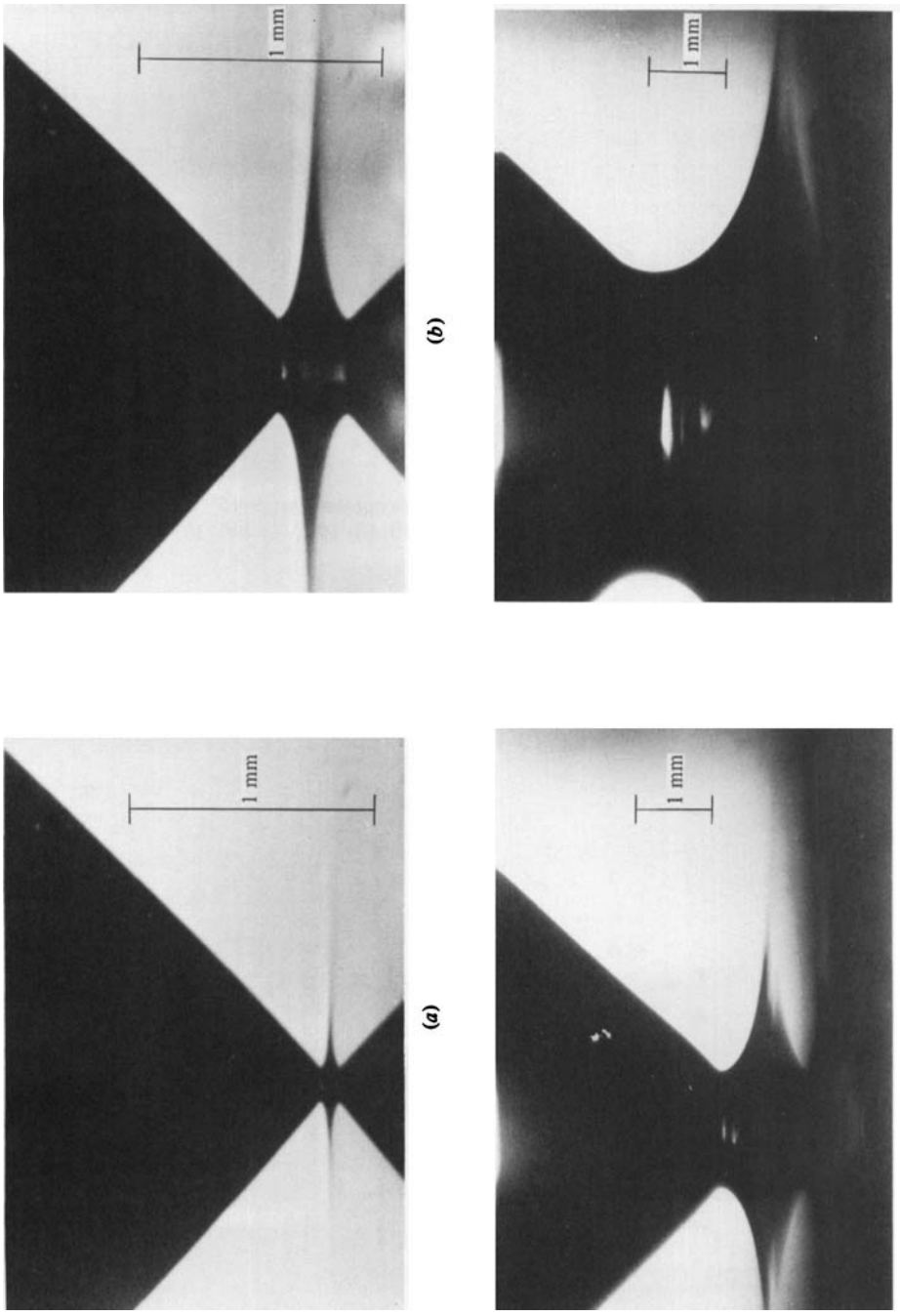

FIGURE 5. Typical photographs of evolving meniscus. $\nu = 10^3$ mm^2 s^{-1}. Cone semi-angle = 45°. (*a*) t = 10 ms; (*b*) 50 ms; (*c*) 250 ms; (*d*) 5 s. Note change of scale.

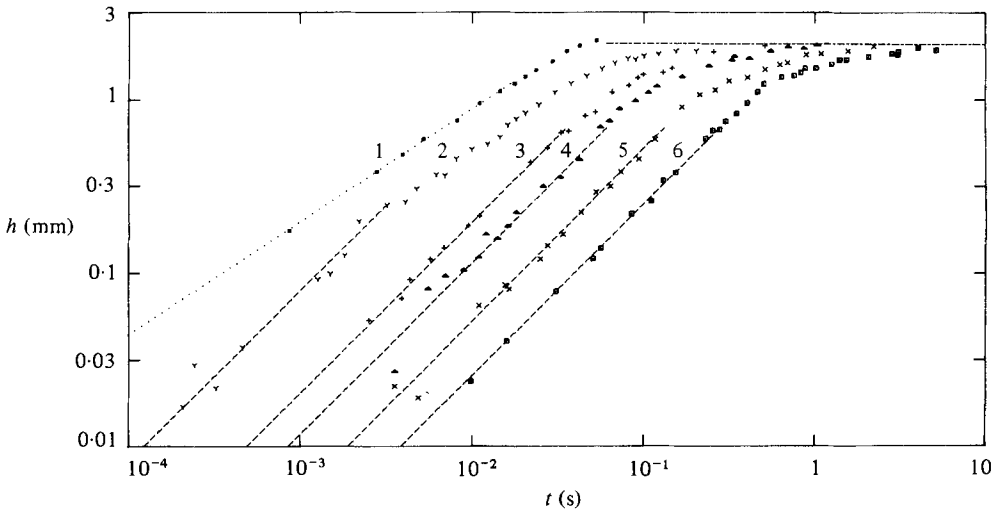

FIGURE 6. Meniscus height h as a function of time for cones having semi-angle 45°. Kinematic-viscosity values (in $mm^2\ s^{-1}$) increase from left to right: (1) 1; (2) 20; (3) 100; (4) 200; (5) 500; (6) 1000. (1) Water; (2)–(6) silicone fluid.

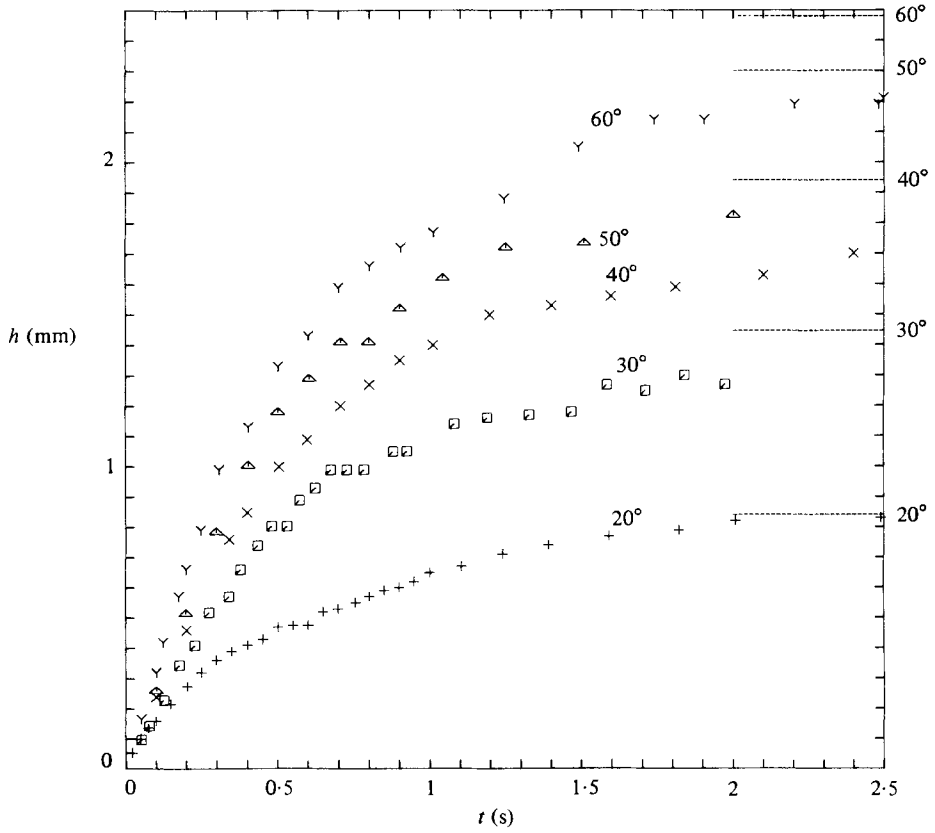

FIGURE 7. Meniscus height as a function of time for cones of varying semi-angle. $\nu = 10^3\ mm^2\ s^{-1}$. The dashed lines at the right indicate the final heights.

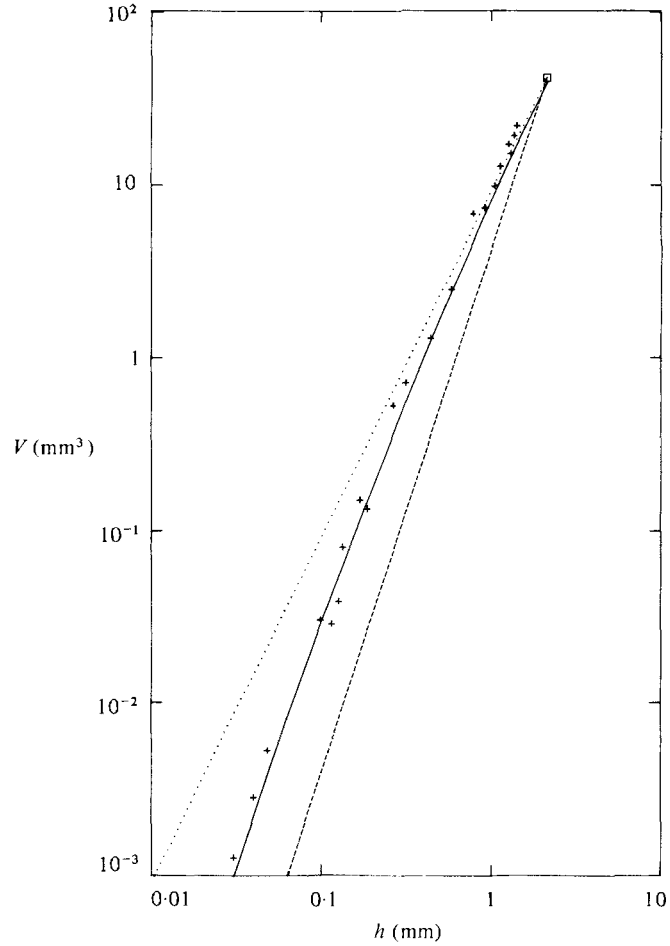

FIGURE 8. Meniscus volume V as a function of height h. $\theta = 45°$; $\nu = 10^3$ mm^2 s^{-1}. +, experimental values; □, calculated value for static meniscus. ....., $V \propto h^2$; ----, $V \propto h^3$; ——, $V = 41h^3/(1+4{\cdot}0h)$. (Dimensions in mm.)

final height, indicating the insignificance of the gravitational term in the governing equation (14). Curves 2 and 3 correspond to lower viscosity values (20 and 100 mm^2 s^{-1} respectively). The effect of inertial terms is apparent here. From (12) Re may be estimated at the upper limit of the linear portion of $h(t)$ in figure 6. The values are about 0·20 for curve 2, and about 0·26 for curve 3. By contrast, for curve 6, $Re \approx 5 \times 10^{-3}$ when $h = 1$ mm. The transition from the viscous limit to the inertial limit thus occurs for viscosity values $\leqslant 100$ mm^2 s^{-1}. For water ($\nu = 1$ mm^2 s^{-1}) the viscous forces are entirely negligible except at the very early stages of meniscus formation. The inertial terms dominate the process until $h \gtrsim 0{\cdot}5h_\infty$. For $0{\cdot}1h_\infty < h < 0{\cdot}8h_\infty$ the dependence of h on t is closely described by

$$h \propto t^{\frac{2}{3}}.$$

Curve 2 shows a transitional case, in which $h \propto t$ initially, changing to $h \propto t^{\frac{2}{3}}$ at $h \approx 0{\cdot}1h_\infty$.

In the viscous limit the initial speed depends on the single unknown parameter b, which is the constant in the equation for the drag coefficient (11). The value of b can

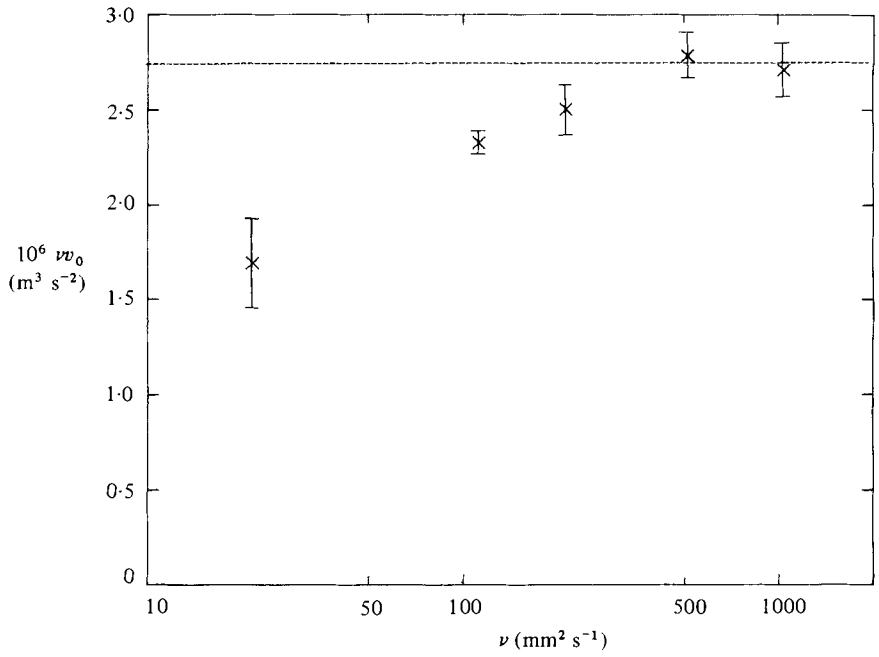

FIGURE 9. Product of initial speed and viscosity plotted against viscosity for $\theta = 45°$, derived from figure 6. The vertical bars are 95% confidence limits. ----, the weighted mean of the two final values.

be derived from the experimental results for $h(t)$. In the viscous limit (19) predicts that

$$v_0 \nu = \frac{8\pi\sigma \cos\theta}{b\rho}, \tag{22}$$

which is a constant for a given liquid and cone. In order to test this prediction $v_0 \nu$ has been plotted against ν for the data in figure 6. v_0 was calculated by linear regression of h against t over the linear portions of curves 2–6. The results are shown in figure 9. They confirm that the viscous limit is effectively attained at viscosity values between 200 and 500 $mm^2\ s^{-1}$.

From (22) and figure 9 the value of b may be deduced for a 45° cone as

$$b = 131 \pm 7.$$

Data for cones having semi-angles between 20° and 60° are shown in figure 7. It has not been possible to repeat measurements for all cone angles at different viscosities, but the results for $\theta = 45°$ discussed above suggest that for $\nu = 10^3\ mm^2\ s^{-1}$ it is valid to assume that the viscosity is dominant, and that (19) may be applied. On this assumption b has been calculated from $h(t)$ for various values of θ. The results are given in figure 10, which shows the remarkable result that $b \tan\theta$ is virtually constant over the range $\theta = 30°$–$60°$, having the value

$$b \tan\theta = 137 \pm 8$$

with 95% confidence. The value for $\theta = 20°$ appears to be significantly higher, but whether this represents a significant trend is uncertain. Unfortunately it is very difficult to obtain good data for cone angles less than 30°, owing to the extremely small size of the meniscus (see figure 7).

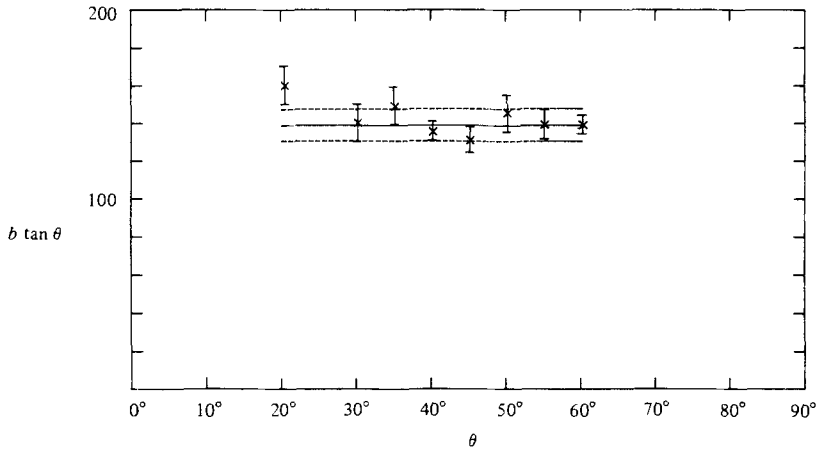

FIGURE 10. $b \tan \theta$ as a function of θ. b is the parameter that determines the drag coefficient (see (11)). ——, weighted mean of the values for $30° < \theta < 60°$; – – – –, 95% confidence limits.

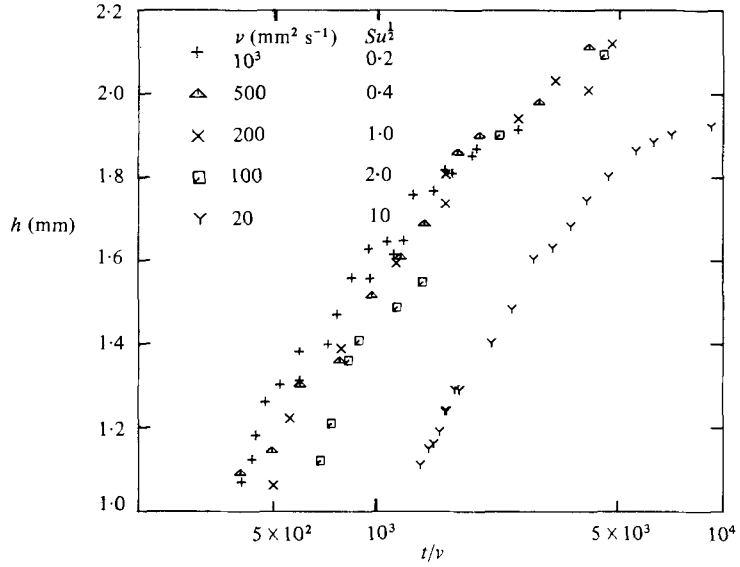

FIGURE 11. Scaled $h(t)$ data for $h > 0{\cdot}5h_\infty$. h is plotted against t/ν. The values of viscosity ν and Suratman number Su are shown in the inset table.

5.2. *Analysis of data for* $h \gtrsim 0{\cdot}5h_\infty$

The behaviour of $h(t)$ when the gravitational term becomes significant is more complicated than the initial behaviour discussed above. As explained in §2.4, the relevant dimensionless group for the viscous limit is the Suratman number $Su = (\sigma^3/g\nu^4\rho^3)^{\frac{1}{2}}$. Since σ and ρ are constant for the liquids used, it is helpful to see how $h(t)$ scales with ν. Figure 11 shows h plotted against t/ν for $h \gtrsim 0{\cdot}5h_\infty$. It is clear from this that similarity exists if t scales as ν; in other words, $Su^{\frac{1}{2}}$ is the appropriate dimensionless group. The critical value of Su for viscous behaviour is about 1, corresponding to $\nu \approx 200$ mm^2 s^{-1}.

5.3. *Attempt to fit the model equation to* $h(t)$

The model proposed in §2 leads to the governing equation (14) for $h(t)$. In the absence of experimental data this equation contains the unknown drag parameter b and the

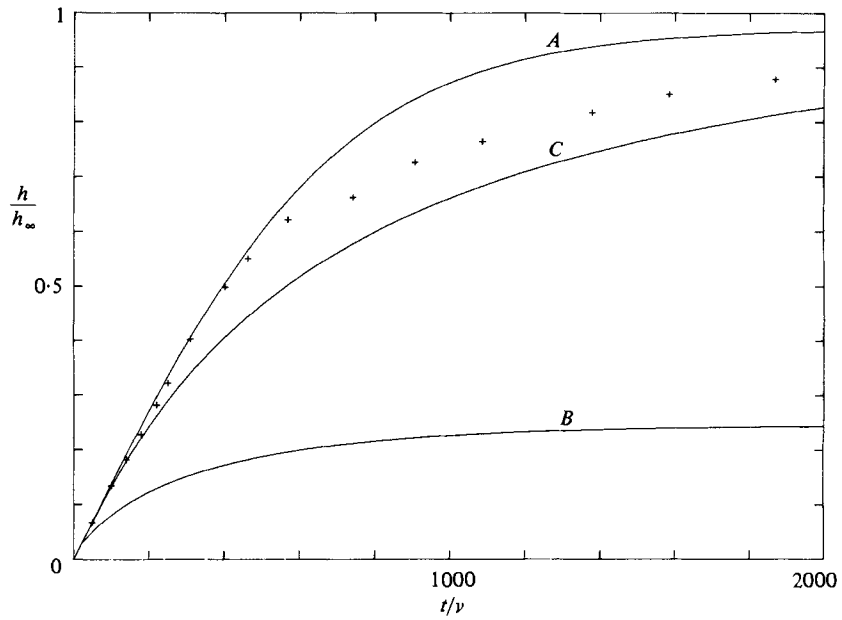

FIGURE 12. Attempts to fit the governing equation (14) to the data. The crosses denote averaged data for several values of viscosity, normalized by plotting h/h_∞ against t/ν. Curve A is $h/h_\infty = \tanh \frac{1}{731} t$. Curve B is obtained by taking $V(h)$ from figure 14, based on static profiles; $\alpha = 0$. Curve C is numerically integrated from (14), with $\alpha = 0$, $b = 131$ and $V = 41h^3/(1+4{\cdot}0h)$.

unknown functions $V(h)$, $\alpha(h)$. The simplest hypotheses suggested in §2.2 are that $V = kh^3$ and $\alpha = 0$ (perfect wetting). These lead to the exact solution (15)

$$h = h_\infty \tanh \frac{t}{\tau},$$

where h_∞ and τ are given by (16) and (17). Since k is known from the static profiles (see appendix) there is only one adjustable parameter b. This may be deduced from the initial rate of rise, as described in §5.1. The solution (15) for $h(t)$ is thus completely determined. It is shown by curve A in figure 12.

The second hypothesis concerning $V(h)$ suggested in §2.2 is that the dynamic profiles differ from the static profiles only very near the contact line. $V(h)$ can then be calculated from the numerically integrated Young–Laplace equation. Figure 14 in the appendix shows the results for $\theta = 45°$. The result of using the $V(h)$ calculated in this way is shown in curve B of figure 12. It is clear that the static profiles greatly exaggerate the volume during the early stages of the process. This may be confirmed by comparing the computed profiles shown in figure 13 with the photographs in figure 5. These show that the dynamic profiles fall off much more rapidly with radius than the static ones. It appears that the surface disturbance propagates radially at a speed significantly lower than the vertical speed (dh/dt).

The third method of incorporating $V(h)$ into (14) is to use the experimental values shown in figure 8. This shows that V is indeed proportional to h^3 at low values of h, but that, as $h \to h_\infty$, $V \propto h^2$. Since it is at the higher values of h that V becomes significant it is likely that an improved fit will be obtained by incorporating the experimental values of $V(h)$ into(14). This can either be done directly or, more conveniently, by choosing an approximating function for $V(h)$. A simple function which fits the data quite well is

$$V = \frac{K_1 h^3}{1 + K_2 h}.$$

It should be noted that K_1 and K_2 are not independent, for when $h = h_\infty$ $V = V_\infty$; i.e.

$$\frac{K_1}{1+K_2 h_\infty} = k,$$

where k is known from the static profiles. Thus

$$K_2 = \frac{1}{h_\infty}\left(\frac{K_1}{k} - 1\right),$$

and, for $\theta = 45°$, $h_\infty = 2{\cdot}13$ mm and $k = 4{\cdot}33$ (see appendix). Therefore $K_2 = 0{\cdot}11K_1 - 0{\cdot}47$ ($\theta = 45°$) when the dimensions are in mm. The best fit to the experimental data in figure 8 consistent with this requirement is given by

$$K_1 = 41, \quad K_2 = 4{\cdot}0.$$

The 95% confidence limits on K_1 are at 54 and 33.

Equation (14) may now be integrated numerically if the contact angle α is taken to be zero, as might be expected for pre-wetted cones. The result of this integration is shown by curve C in figure 12.

It is apparent from figure 12 that the inclusion of experimental values of $V(h)$ does not give a particularly good fit to the experimental $h(t)$ data. The gravitational term is plainly large enough to reduce the rate of rise appreciably at less than half the final height, whereas the actual rate is almost constant up to this stage.

Any further improvements to the fit between (14) and the experimental data must await more detailed information about the behaviour in the immediate vicinity of the contact line. This might enable α to be included in a more satisfactory manner than the present assumption that $\alpha = 0$ throughout the process. In the meantime the model provides a useful first approximate description of the process which satisfactorily accounts for several important features.

6. Conclusions

A simple model has been formulated to describe the evolution of a liquid meniscus on a cone in the viscous limit ($Re \ll 1$, $Su \lesssim 1$). The model describes the drag force by a single adjustable parameter applicable to cones of any semi-angle between 30° and 60°, and to liquids of viscosity $\gtrsim 200$ mm^2 s^{-1}. The meniscus shape is incorporated either by ad hoc methods or by using experimental data.

Detailed experimental results have been presented for the variation of meniscus height with time for prewetted cones having semi-angles between 20° and 60° and for liquid viscosities in the range 1–10^3 mm^2 s^{-1}. The main features of the results are satisfactorily accounted for by the model. However, a close fit to the experimental results requires knowledge of the effective contact-angle variation during the evolution of the meniscus.

My grateful thanks are due to John Acton for many helpful discussions. Miklos Tatar meticulously developed all the films. Finally, I am most grateful to the School of Physics, University of Bath, for affording the facilities for this work.

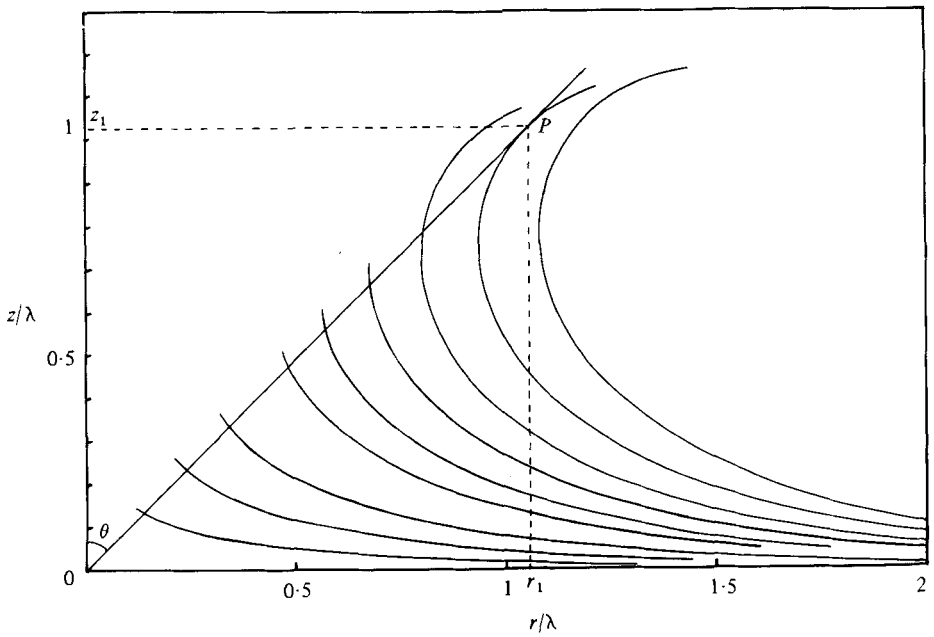

FIGURE 13. Static meniscus profiles obtained numerically. The scale are normalized to the capillary constant. r_1, z_1 are the coordinates of the circle of contact through the point P on a cone having semi-angle $\theta = 45°$.

Appendix

Static meniscus profiles

The shape of static axisymmetric meniscus profiles may be found by numerical integration of the Young–Laplace equation

$$\frac{1}{R_1}+\frac{1}{R_2}=\frac{p}{\sigma},$$

where R_1 and R_2 are the principal radii of curvature. The method adopted here is based on that of Freud & Freud (1930) (see also Huh & Scriven 1969). The integration, performed here by a Runge–Kutta technique, produces a family of profiles, each starting at the free surface and terminating at a point on the contacting cone, such that (for zero contact angle) $dz/dx = z/x$ (see figure 13). Similar results have been published by Hartland & Hartley (1976).

From such a family of profiles a graph may be drawn of the height of the circle of contact as a function of cone angle. From this graph it may be found that, for $\theta = 45°$,

$$h_\infty = 1{\cdot}01\lambda,$$

where λ is the capillary constant $(2\sigma/\rho g)^{\frac{1}{2}}$. For $\rho = 971$ kg m^{-3} and $\sigma = 21{\cdot}2$ mN m^{-1} this gives $h_\infty = 2{\cdot}13$ mm.

Volume of the static meniscus

The volume contained between the free surface, the cone and the static meniscus surface is given by (Freud & Freud 1930)

$$V = (\pi r_1^2 z_1 + \pi u_1 r_1 - \tfrac{1}{3}\pi \tan^2\theta\, r_1^3)\lambda^3,$$

where r_1, z_1 are coordinates of the contact line, and $u_1 = \sin\{\tan^{-1}(dz/dr)\}$ at the contact line.

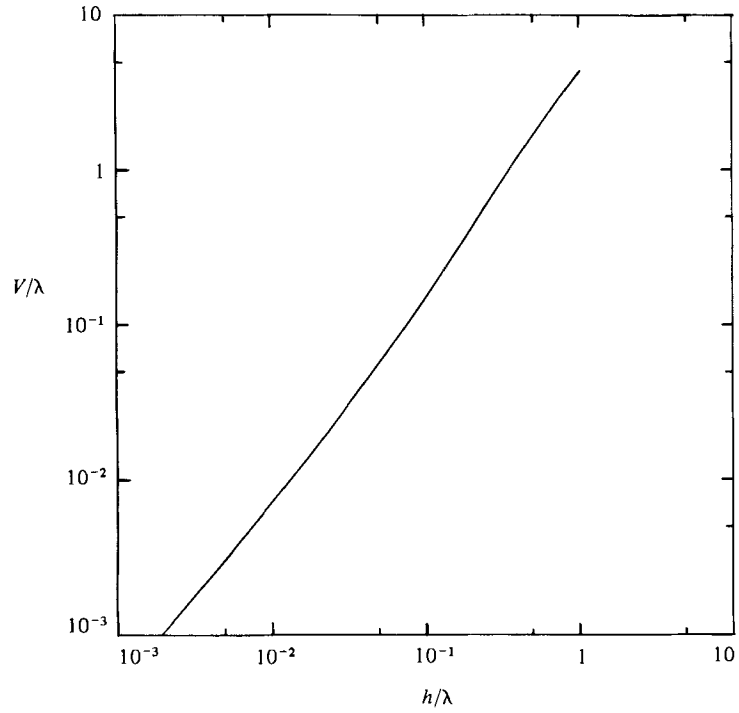

FIGURE 14. Meniscus volume as a function of height calculated from the static profiles. $\theta = 45°$, $\lambda = 2{\cdot}11$ mm. (Compare figure 8.)

The values of r_1, z_1 and u_1 can be found for any cone angle θ and height h from the computed profiles. Hence $V(h)$ can be found. The results for $\theta = 45°$, $\lambda = 2{\cdot}11$ mm, are shown in figure 14. For the range of h over which $V(h)$ is significant in (14), it may be adequately represented by

$$V = 14{\cdot}4h^{1{\cdot}44}.$$

This should be contrasted with the empirical data shown in figure 8 and discussed in §5.3. The two estimates of V agree at the final height $h_\infty = 2{\cdot}13$ mm. It follows that the constant k in (5) must be such that (in units of mm)

$$V_\infty = kh_\infty^3 = 14{\cdot}4h_\infty^{1{\cdot}44},$$

$$\therefore k = 4{\cdot}33.$$

Volume of the dynamic meniscus

The volume of the meniscus as a function of height is shown in figure 8. The method of calculation of the volume V from the profiles is based on Pappus's theorem. The geometry is shown in figure 15.

We have

$$V = 2\pi A r_c,$$

where A is the area of the plane axial section OPS, shaded in figure 15, and r_c is the radial coordinate of the centroid of A. It is easily shown that

$$V = 2\pi \oint rz\, dr,$$

where the line integral is taken around OPS. This integral may be conveniently evaluated using a digitizing table interfaced to a computer.

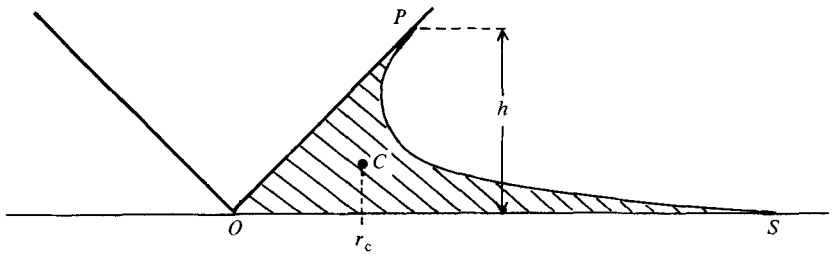

FIGURE 15. Diagram of the meniscus, defining the geometry for evaluating the meniscus volume V. C is the centroid of area of the section OPS, and r_c the radial coordinate of C.

REFERENCES

BASHFORTH, F. & ADAMS, J. C. 1883 *An Attempt to Test the Theory of Capillary Action.* Cambridge University Press.

BIKERMAN, J. J. 1970 *Physical Surfaces.* Physical Chemistry vol. 20. Academic.

CATCHPOLE, J. P. & FULFORD, G. 1966 Dimensionless groups. *Ind. Engng Chem.* **58**, 46–60.

DUSSAN, V., E. B. 1979 On the spreading of liquids on solid surfaces: static and dynamic contact lines. *Ann. Rev. Fluid Mech.* **11**, 371–400.

FREUD, B. & FREUD, B. B. 1930 A theory of the ring method for the determination of surface tension. *J. Am. Chem. Soc.* **52**, 1772–1781.

HANSEN, R. J. & TOONG, T. Y. 1971 Dynamic contact angle and its relationship to forces of hydrodynamic origin. *J. Colloid Interface Sci.* **37**, 196–207.

HARTLAND, S. & HARTLEY, R. W. 1976 *Axisymmetric Fluid–Liquid Interfaces.* Elsevier.

HUH, C. & MASON, S. G. 1977 The steady movement of a liquid meniscus in a capillary tube. *J. Fluid Mech.* **81**, 401–419.

HUH, C. & SCRIVEN, L. E. 1969 Shapes of axisymmetric fluid interfaces of unbounded extent. *J. Colloid Interface Sci.* **30**, 323–337.

KISSLING, R. L. & GROSS, P. H. 1970 Capillary behaviour of viscous liquids. *J. Phys. Chem.* **74**, 318–326.

MAY, A. & WOODHULL, J. C. 1948 Drag coefficients of steel spheres entering water vertically. *J. Appl. Phys.* **19**, 1109–1121.

MILOH, T. 1981 Wave slam on a sphere penetrating a free surface. *J. Engng Math.* **15**, 221–240.

MOGHISI, M. & SQUIRE, P. T. 1981 An experimental investigation of the initial force of impact on a sphere striking a liquid surface. *J. Fluid Mech.* **108**, 133–146.

PADDAY, J. F. 1976 The equilibrium and stability properties of menisci: the measurement of surface tension by exact methods. *Pure Appl. Chem.* **48**, 485–494.

SHIFFMAN, M. & SPENCER, D. C. 1951 The force of impact on a cone striking a water surface. *Communs Pure Appl. Math.* **4**, 379–417.

WATANABE, S. 1930 Resistance of impact on a water surface. Part I – Cone. *Inst. Phys. Chem. Res., Tokyo Sci. Papers* **226**, 251–267.